

Weakly Nonlinear Analysis of Electroconvection in a Suspended Fluid Film

V.B. Deyirmenjian, Zahir A. Daya, and Stephen W. Morris

Department of Physics and Erindale College,

University of Toronto, Toronto, Ontario, Canada, M5S 1A7

(October 31, 2018)

Abstract

It has been experimentally observed that weakly conducting suspended films of smectic liquid crystals undergo electroconvection when subjected to a large enough potential difference. The resulting counter-rotating vortices form a very simple convection pattern and exhibit a variety of interesting nonlinear effects. The linear stability problem for this system has recently been solved. The convection mechanism, which involves charge separation at the free surfaces of the film, is applicable to any sufficiently two-dimensional fluid. In this paper, we derive an amplitude equation which describes the weakly nonlinear regime, by starting from the basic electrohydrodynamic equations. This regime has been the subject of several recent experimental studies. The lowest order amplitude equation we derive is of the Ginzburg-Landau form, and describes a forward bifurcation as is observed experimentally. The coefficients of the amplitude equation are calculated and compared with the values independently deduced from the linear stability calculation.

Typeset using REVTeX

I. INTRODUCTION

Although spatio-temporal pattern formation is ubiquitous in nature, there are relatively few systems which are amenable to both accurate experimental study and first-principles weakly nonlinear analysis. [1] The classic examples involving fluid mechanical instabilities are Rayleigh-Bénard convection and Taylor-Couette flow. The results of perturbation theory based on the Navier-Stokes and heat equations are in good agreement with high precision experiments in the weakly nonlinear regime of these two instabilities. [1,2] A more complex example is electroconvection in nematic liquid crystals due to the Carr-Helfrich mechanism. [3] Here, remarkably good agreement has been achieved in spite of the complexity of the problem. However, in other cases either the materials cannot be sufficiently characterized or the underlying physical equations are not understood well enough to allow quantitative comparisons between observations and theory.

Electroconvection in suspended smectic films is a promising new experimental system for quantitative studies of spatio-temporal pattern formation. [4–7] When a thin, suspended film of smectic liquid crystal is subjected to a sufficient potential difference, a charge separation arises which drives the film into convection. The flow pattern just above onset is sustained by the electric field acting on charges which develop near the free surfaces of the film. These charges are simply a consequence of the electrostatic boundary conditions which must be satisfied by the fields inside and outside of the film. [8] Fig. 1 shows a schematic of the experimental arrangement. This source of charge is distinct from that due to the Carr-Helfrich mechanism which drives bulk electroconvection in certain nematics. [3] In that case, the charge generation mechanism involves an essential coupling to the director orientation. In experiments on smectic A liquid crystal films [4–7], in which the director was perpendicular to the film, no orientational effects were observed, indicating that the flow remained isotropic in the film plane. Recent experiments on smectic C films [9] showed convection and flow alignment of the projection of the director in the plane of the film, but were not consistent with the Carr-Helfrich mechanism. These were likely driven by the mechanism discussed

here, with the flow alignment a secondary effect. It has, however, been hypothesized [10] that the two mechanisms might coexist in some smectic C materials. The mechanism we discuss here is presumably also responsible for convection observed in thin, suspended films of isotropic fluids and in nematics in certain regimes [11]. These cases involve substantial three-dimensional effects, however, because they lack the smectic layering which has the effect of restricting the flow to the film plane. In what follows, we consider only very thin isotropic films, relevant to the case of smectic A, on which most of the experiments have been performed. [4–7]

A theoretical model of the onset of electroconvection in suspended films was introduced by Daya, Morris, and de Bruyn. [8] The film was represented as a weakly conducting, two-dimensional, isotropic fluid. To find the electric fields and charge densities which drive convection, the electrostatic potential was determined. The three-dimensional electrostatic equations effectively constitute a nonlocal coupling between the in-plane fields and charge densities which appear in the two-dimensional Navier-Stokes and charge continuity equations. This extra coupling formally distinguishes the resulting equations from those of thermal convection in the Rayleigh-Bénard problem, although some interesting similarities remain. The value of the critical wavenumber from the linear stability analysis [8] is in good agreement with experiment [4,5,7].

The purpose of this paper is to present a weakly nonlinear analysis of the electrohydrodynamic equations given in Ref. [8]. The multiple-scales perturbation theory employed in our treatment is similar to that given in Ref. [1] for Rayleigh-Bénard convection. Although there are important physical differences between these two pattern forming instabilities, the resulting amplitude equation for both problems is of the Ginzburg-Landau form

$$\tau_0 \partial_t A = \epsilon A + \xi_0^2 \partial_x^2 A - g_0 A |A|^2, \quad (1.1)$$

where ϵ is the control parameter, which depends on the applied electric potential, and $A(x, t)$ is a slowly varying amplitude. The coefficients τ_0 , ξ_0 , and g_0 are compared with those previously obtained by other methods. In particular, τ_0 and ξ_0 are found to be in

good agreement with the values determined from the linear stability analysis of Daya *et al.* [8] Mao, de Bruyn, and Morris have experimentally measured all three coefficients. [7] The experimental value of ξ_0 is in reasonable agreement with theory. Quantitative comparison of τ_0 and g_0 with theory is difficult at the present time due to large uncertainties in the conductivity and viscosity of the liquid crystal, which are required to non-dimensionalize the experimental results.

Determining the amplitude equation constitutes a first step towards understanding the fully nonlinear regime beyond the onset of electroconvection. For small wavenumbers near threshold, the stability of solutions of Eqn. 1.1 determines the regions of control parameter-wavenumber space where the vortex pattern itself is stable. [1] For example, one expects such a one-dimensional pattern to exhibit a long-wavelength instability due to the Eckhaus mechanism [1,12] which restricts the range of stable wavenumbers available to the pattern. The amplitude equation can also be used to study how the ends of a finite-length film affect the range of stable wavenumbers. This wavenumber selection mechanism was first investigated by Cross, Daniels, Hohenberg, and Siggia [13] in the context of Rayleigh-Bénard convection in finite containers. End-selection was observed experimentally by Mao, Morris, Daya, and de Bruyn [6] in electroconvection patterns in smectic A films. It is possible to extend the present theory to determine the Eckhaus and end-selection stability boundaries [14], but this is beyond the scope of the present paper.

This paper is organized as follows. The linear stability analysis of the electroconvective instability is briefly reviewed in Section II. The amplitude equation is determined in Section III. Section IV compares the results of this theoretical investigation with previously obtained observations, and contains a brief conclusion.

II. LINEAR STABILITY ANALYSIS

In this section, the physical model describing electroconvection in a thin film is presented. The linear stability analysis of the relevant equations is concisely reviewed. Further details

are given in Ref. [8]. Note that we change some of the notation of Ref. [8] to simplify the presentation of this paper.

The film is treated as a two-dimensional conducting fluid in the xy -plane, with areal material parameters $\rho_s = s\rho$, $\eta_s = s\eta$, and $\sigma_s = s\sigma$, where s , ρ , η , and σ are the film thickness, bulk density, bulk molecular viscosity, and bulk conductivity, respectively. The coordinate system is shown in Fig. 1. The film is assumed to be infinite in the x -direction and bounded between $-d/2$ and $d/2$ in the y -direction. We only consider the thin film limit where $s/d \rightarrow 0$. Two electrode configurations are analyzed. In the ‘plate’ geometry, the film is suspended between two thin sheet electrodes which fill the rest of the xy plane, whereas in the ‘wire’ geometry, the film is suspended between two thin line electrodes which are along the x direction. In both cases, the electrode at $y = -d/2$ is fixed at a potential of $-V/2$, and the electrode at $y = d/2$ is at a potential of $V/2$.

The Navier-Stokes equation

$$\rho_s \left[\frac{\partial \mathbf{u}}{\partial t} + (\mathbf{u} \cdot \nabla_s) \mathbf{u} \right] = -\nabla_s P_s + \eta_s \nabla_s^2 \mathbf{u} + q \mathbf{E}_s, \quad (2.1)$$

describes the fluid flow of the liquid crystal, where $\nabla_s = (\partial_x, \partial_y, 0)$, $P_s(x, y)$, $q(x, y)$, and $\mathbf{E}_s(x, y)$ are the two-dimensional gradient operator, two-dimensional pressure field, surface charge density, and electric field in the film plane, respectively. The incompressibility of the fluid implies that

$$\partial_x u + \partial_y v = 0, \quad (2.2)$$

where $u(x, y)$ and $v(x, y)$ are the x and y components of the two-dimensional velocity field \mathbf{u} . The pressure field is eliminated from Eqn. 2.1 by applying the curl operator. Taking the curl of Eqn. 2.1 twice, using Eqn. 2.2, and selecting the y component gives:

$$\begin{aligned} & -\rho_s \partial_t \nabla_s^2 v + \rho_s \partial_y (\nabla_s \cdot [(\mathbf{u} \cdot \nabla_s) \mathbf{u}]) - \rho_s \nabla_s^2 [(\mathbf{u} \cdot \nabla_s) v] = \\ & -\eta_s \nabla_s^4 v + (\partial_x^2 q)(\partial_y \Psi|_{z=0}) + (\partial_x q)(\partial_{xy} \Psi|_{z=0}) - (\partial_{xy} q)(\partial_x \Psi|_{z=0}) - (\partial_y q)(\partial_x^2 \Psi|_{z=0}) \quad , \quad (2.3) \end{aligned}$$

where the electric potential $\Psi(x, y, z)$ is related to the in-plane electric field via $\mathbf{E}_s(x, y) = -\nabla_s \Psi(x, y, z)|_{z=0}$. The three-dimensional Laplace equation,

$$\nabla^2 \Psi = 0, \quad (2.4)$$

specifies Ψ in the half space $z \geq 0$ with appropriate boundary conditions in the xy -plane, where $\nabla = (\partial_x, \partial_y, \partial_z)$. The surface charge density depends on the discontinuity in the z -derivative of Ψ across the two surfaces of the film:

$$\begin{aligned} q &= -\epsilon_0 \frac{\partial \Psi}{\partial z} \Big|_{z=0^+} + \epsilon_0 \frac{\partial \Psi}{\partial z} \Big|_{z=0^-}, \\ &= -2\epsilon_0 \frac{\partial \Psi}{\partial z} \Big|_{z=0^+}, \end{aligned} \quad (2.5)$$

where ϵ_0 is the permittivity of free space.

The motion of charge is governed by the charge continuity equation

$$\frac{\partial q}{\partial t} = -\nabla_s \cdot (q\mathbf{u} + \sigma_s \mathbf{E}_s), \quad (2.6)$$

which includes contributions from both the conductive $\sigma_s \mathbf{E}_s(x, y)$ and convective $q(x, y)\mathbf{u}(x, y)$ current densities. Diffusion of charge in the plane of the film can be neglected.

Equations 2.3-2.6 constitute the basic electrohydrodynamic equations; the electrode geometry enters into the boundary conditions on Ψ . The solution of these equations in the “base state” below the onset of convection has $\mathbf{u}^{(0)}(x, y) = 0$, with $q^{(0)}(y)$ and $\Psi^{(0)}(y, z)$ satisfying the electrostatic boundary value problem given by Eqns. 2.4 and 2.5. To examine the stability of the base state, we introduce the perturbed quantities

$$\mathbf{u} = 0 + \mathbf{u}^{(1)}, \quad (2.7)$$

$$q = q^{(0)} + q^{(1)}, \quad (2.8)$$

$$\mathbf{E}_s = \mathbf{E}_s^{(0)} + \mathbf{E}_s^{(1)}, \quad (2.9)$$

where $\mathbf{E}_s^{(0)} = E_y^{(0)}\hat{\mathbf{y}}$ and $\mathbf{E}_s^{(1)}(x, y) = E_x^{(1)}(x, y)\hat{\mathbf{x}} + E_y^{(1)}(x, y)\hat{\mathbf{y}}$. Quantities which have dimensions of length, time, charge density, and electric potential are nondimensionalized by d , $\epsilon_0 d/\sigma_s$, $\epsilon_0 V/d$, and V , respectively. Substituting the perturbed field variables into Eqns. 2.3-2.6, nondimensionalizing, and suppressing the superscripts, yields

$$\begin{aligned} \nabla_s^4 v - \mathcal{R} \partial_x^2 q + \mathcal{R} Q \partial_x^2 \Psi|_{z=0} &= \mathcal{R} \partial_x [(\partial_x q)(\partial_y \Psi|_{z=0}) - (\partial_y q)(\partial_x \Psi|_{z=0})] \\ + \mathcal{P}^{-1} \{ \partial_t (\nabla_s^2 v) - \partial_y (\nabla_s \cdot [(\mathbf{u} \cdot \nabla_s) \mathbf{u}]) + \nabla_s^2 [(\mathbf{u} \cdot \nabla_s) v] \}, \end{aligned} \quad (2.10)$$

$$-Qv + \nabla_s^2 \Psi|_{z=0} = \partial_t q + u(\partial_x q) + v(\partial_y q), \quad (2.11)$$

$$q + (\partial_z \Psi)|_{z=0^+} - (\partial_z \Psi)|_{z=0^-} = 0, \quad (2.12)$$

$$\nabla^2 \Psi = 0. \quad (2.13)$$

The dimensionless parameters \mathcal{R} and \mathcal{P} are analogous to the Rayleigh and Prandtl numbers. We will henceforth consider only the limit $\mathcal{P} \rightarrow \infty$, as this is the case most relevant to experiments on real smectic materials [7], for which $\mathcal{P} \approx 10 - 100$. The non-constant coefficient $Q(y)$ depends on the electrode configuration and is given by $Q(y) = \partial_y q^{(0)}(y)$, where $q^{(0)}(y)$ is the base state charge density. The variables v , q , and Ψ above represent the dimensionless perturbed functions $v^{(1)}$, $q^{(1)}$, and $\Psi^{(1)}$, respectively, and satisfy the following boundary conditions:

$$v(x, y = \pm \frac{1}{2}) = (\partial_y v)(x, y = \pm \frac{1}{2}) = 0, \quad (2.14)$$

$$\Psi(x, y = \pm \frac{1}{2}, 0) = 0, \quad (2.15)$$

$$\Psi(x, y, z) \rightarrow 0, \quad z \rightarrow \pm \infty. \quad (2.16)$$

In the plate electrode configuration, Dirichlet boundary conditions are employed on the xy plane, with

$$\Psi(x, y, 0) = 0, \quad |y| > \frac{1}{2}. \quad (2.17)$$

In the wire electrode geometry, mixed boundary conditions apply such that

$$\partial_z \Psi(x, y, z)|_{z=0^+} = 0, \quad |y| > \frac{1}{2}. \quad (2.18)$$

In both cases the potential $\Psi(x, y, 0) = \Psi|_{z=0}(x, y)$, $|y| \leq \frac{1}{2}$, is specified on the film.

Equations 2.10-2.13 can be expressed as

$$\mathcal{L}\mathcal{C} = \mathcal{B} , \quad (2.19)$$

where

$$\mathcal{L} = \begin{pmatrix} \nabla_s^4 & -\mathcal{R}\partial_x^2 & \mathcal{R}Q\partial_x^2 & 0 \\ -Q & 0 & \nabla_s^2 & 0 \\ 0 & 1 & 0 & \partial_z(\cdot)|_{z=0^+} - \partial_z(\cdot)|_{z=0^-} \\ 0 & 0 & 0 & \nabla^2 \end{pmatrix}, \quad (2.20)$$

$$\mathcal{C} = \begin{pmatrix} v(x, y) \\ q(x, y) \\ \Psi(x, y, z)|_{z=0} \\ \Psi(x, y, z) \end{pmatrix}, \quad (2.21)$$

and

$$\mathcal{B} = \begin{pmatrix} \mathcal{R}\partial_x[(\partial_x q)(\partial_y \Psi|_{z=0}) - (\partial_y q)(\partial_x \Psi|_{z=0})] \\ \partial_t q + u(\partial_x q) + v(\partial_y q) \\ 0 \\ 0 \end{pmatrix}. \quad (2.22)$$

The linear stability problem is defined by

$$\mathcal{L}\mathcal{C} = 0 . \quad (2.23)$$

The neutral stability curve $\mathcal{R} = \mathcal{R}_c(\kappa)$ is determined by substituting the normal mode solution

$$\mathcal{C} = \begin{pmatrix} \bar{v}_\kappa(y) \\ \bar{q}_\kappa(y) \\ \bar{\Psi}_\kappa(y, 0) \\ \bar{\Psi}_\kappa(y, z) \end{pmatrix} e^{i\kappa x} = \bar{\mathcal{C}}_\kappa e^{i\kappa x}, \quad (2.24)$$

into Eqn. 2.23. The following alterations have been made to the notation of Ref. [8]: $\Lambda(y) \rightarrow \bar{v}_\kappa(y)$, $\Theta(y) \rightarrow \bar{q}_\kappa(y)$, $\Omega_s(y) \rightarrow \bar{\Psi}_\kappa(y, 0)$, and $\Omega(y, z) \rightarrow \bar{\Psi}_\kappa(y, z)$. The variables \bar{v}_κ , \bar{q}_κ , and $\bar{\Psi}_\kappa$ are expanded as

$$\bar{v}_\kappa(y) = \sum_{m=1}^{\infty} \bar{A}_m \bar{v}_{\kappa m}(y) , \quad (2.25)$$

$$\bar{q}_\kappa(y) = \sum_{m=1}^{\infty} \bar{A}_m \bar{q}_{\kappa m}(y) , \quad (2.26)$$

$$\bar{\Psi}_\kappa(y, z) = \sum_{m=1}^{\infty} \bar{A}_m \bar{\Psi}_{\kappa m}(y, z) , \quad (2.27)$$

where $\bar{v}_{\kappa m}(y)$, $\bar{q}_{\kappa m}(y)$, and $\bar{\Psi}_{\kappa m}(y, z)$ satisfy the boundary conditions Eqns. 2.14 to 2.18. The linear problem is solved numerically in Ref. [8] by substituting C_m , the even Chandrasekhar function [16], for $\bar{v}_{\kappa m}(y)$ and then finding self-consistent solutions for $\bar{q}_{\kappa m}(y)$ and $\bar{\Psi}_{\kappa m}(y, z)$.

III. DERIVATION OF THE AMPLITUDE EQUATION

The multiple-scales approach is used to obtain the amplitude equation, which describes the slow temporal and spatial variation of the field variables. [1,12] The slow scales $X = \epsilon^{1/2}x$ and $T = \epsilon t$ are treated as independent of the fast scales x and t . We choose $\epsilon = (\mathcal{R} - \mathcal{R}_{c0})/\mathcal{R}_{c0}$, where \mathcal{R}_{c0} is the critical value of \mathcal{R} at the minimum of the neutral stability curve $\mathcal{R} = \mathcal{R}_c(\kappa)$. The nonlinear equation describing the system, Eqn. 2.19, is expanded in powers of $\epsilon^{1/2}$ as follows:

$$\mathcal{L} = \mathcal{L}_0 + \epsilon^{1/2}\mathcal{L}_1 + \epsilon\mathcal{L}_2 + \dots , \quad (3.1)$$

$$\mathcal{C} = \epsilon^{1/2}\mathcal{C}_0 + \epsilon\mathcal{C}_1 + \epsilon^{3/2}\mathcal{C}_2 + \dots , \quad (3.2)$$

$$\mathcal{B} = \epsilon^{1/2}\mathcal{B}_0 + \epsilon\mathcal{B}_1 + \epsilon^{3/2}\mathcal{B}_2 + \dots , \quad (3.3)$$

and

$$v(x, y) = \epsilon^{1/2}v_0(x, y) + \epsilon v_1(x, y) + \epsilon^{3/2}v_2(x, y) + \dots , \quad (3.4)$$

$$q(x, y) = \epsilon^{1/2}q_0(x, y) + \epsilon q_1(x, y) + \epsilon^{3/2}q_2(x, y) + \dots , \quad (3.5)$$

$$\Psi(x, y, z) = \epsilon^{1/2}\Psi_0(x, y, z) + \epsilon\Psi_1(x, y, z) + \epsilon^{3/2}\Psi_2(x, y, z) + \dots . \quad (3.6)$$

The differentials ∂_x and ∂_t in the original equations transform as $\partial_x \rightarrow \partial_x + \epsilon^{1/2}\partial_X$ and $\partial_t \rightarrow \partial_t + \epsilon\partial_T$.

At orders $\epsilon^{1/2}$, ϵ , and $\epsilon^{3/2}$, Eqn. 2.19 becomes

$$\mathcal{L}_0 \mathcal{C}_0 = \mathcal{B}_0 , \quad (3.7)$$

$$\mathcal{L}_0 \mathcal{C}_1 + \mathcal{L}_1 \mathcal{C}_0 = \mathcal{B}_1 , \quad (3.8)$$

$$\mathcal{L}_0 \mathcal{C}_2 + \mathcal{L}_1 \mathcal{C}_1 + \mathcal{L}_2 \mathcal{C}_0 = \mathcal{B}_2 , \quad (3.9)$$

respectively.

The most general solution of Eqn. 3.7, at order $\epsilon^{1/2}$, is

$$\mathcal{C}_0 = \begin{pmatrix} v_0(x, y) \\ q_0(x, y) \\ \Psi_0(x, y, z)|_{z=0} \\ \Psi_0(x, y, z) \end{pmatrix} = A_0(X, T) \begin{pmatrix} \bar{v}_0(y) \\ \bar{q}_0(y) \\ \bar{\Psi}_0(y, 0) \\ \bar{\Psi}_0(y, z) \end{pmatrix} e^{i\kappa_0 x} + c.c. , \quad (3.10)$$

where $A_0(X, T)$ is the amplitude function, κ_0 is the critical wavenumber which minimizes the function $\mathcal{R}_c(\kappa)$, and *c.c.* denotes complex conjugation. The functions $\bar{v}_0(y) = \bar{v}_\kappa(y)|_{\kappa=\kappa_0}$, $\bar{q}_0(y) = \bar{q}_\kappa(y)|_{\kappa=\kappa_0}$, and $\bar{\Psi}_0(y, z) = \bar{\Psi}_\kappa(y, z)|_{\kappa=\kappa_0}$ are solutions of the linear stability problem, Eqns. 2.23, 2.24-2.27.

To solve the order ϵ equation, Eqn. 3.8, the relation

$$\frac{\partial}{\partial \kappa} \left[\mathcal{L} \begin{pmatrix} \bar{v}_\kappa(y) e^{i\kappa x} \\ \bar{q}_\kappa(y) e^{i\kappa x} \\ \bar{\Psi}_\kappa(y, 0) e^{i\kappa x} \\ \bar{\Psi}_\kappa(y, z) e^{i\kappa x} \end{pmatrix} \right]_{\kappa=\kappa_0} = 0 , \quad (3.11)$$

is employed. This is used to transform Eqn. 3.8 to

$$\mathcal{L}_0 \tilde{\mathcal{C}}_1 = \mathcal{B}_1 , \quad (3.12)$$

which is solved by the ansatz

$$\tilde{\mathcal{C}}_1 \equiv \begin{pmatrix} \tilde{v}_1(x, y) \\ \tilde{q}_1(x, y) \\ \tilde{\Psi}_1(x, y, 0) \\ \tilde{\Psi}_1(x, y, z) \end{pmatrix}$$

$$= \left\{ \begin{pmatrix} v_1^\epsilon(y) \\ q_1^\epsilon(y) \\ \Psi_1^\epsilon(y, 0) \\ \Psi_1^\epsilon(y, z) \end{pmatrix} A_0^2 e^{2i\kappa_0 x} + \begin{pmatrix} \bar{v}_0(y) \\ \bar{q}_0(y) \\ \bar{\Psi}_0(y, 0) \\ \bar{\Psi}_0(y, z) \end{pmatrix} A_1 e^{i\kappa_0 x} + c.c. \right\} + \begin{pmatrix} v_2^\epsilon(y) \\ q_2^\epsilon(y) \\ \Psi_2^\epsilon(y, 0) \\ \Psi_2^\epsilon(y, z) \end{pmatrix} |A_0|^2. \quad (3.13)$$

The variable $A_1(X, T)$ is a second amplitude function. Substitution of Eqn. 3.13 into Eqn. 3.12 gives the following sets of partial differential equations

$$(\partial_y^2 - (2\kappa_0)^2)v_1^\epsilon + (2\kappa_0)^2 \mathcal{R}_{c0} q_1^\epsilon - (2\kappa_0)^2 \mathcal{R}_{c0} Q \Psi_1^\epsilon|_{z=0} = -2\kappa_0^2 \mathcal{R}_{c0} [\bar{q}_0 (\partial_y \bar{\Psi}_0|_{z=0}) - (\partial_y \bar{q}_0) \bar{\Psi}_0|_{z=0}], \quad (3.14)$$

$$-Q v_1^\epsilon + (\partial_y^2 - (2\kappa_0)^2) \Psi_1^\epsilon|_{z=0} = i\kappa_0 \bar{u}_0 \bar{q}_0 + \bar{v}_0 (\partial_y \bar{q}_0), \quad (3.15)$$

$$q_1^\epsilon + (\partial_z \Psi_1^\epsilon)|_{z=0^+} - (\partial_z \Psi_1^\epsilon)|_{z=0^-} = 0, \quad (3.16)$$

$$(\partial_y^2 + \partial_z^2 - (2\kappa_0)^2) \Psi_1^\epsilon = 0, \quad (3.17)$$

and

$$\partial_y^4 v_2^\epsilon = 0, \quad (3.18)$$

$$-Q v_2^\epsilon + \partial_y^2 \Psi_2^\epsilon|_{z=0} = -i\kappa_0 \bar{u}_0 \bar{q}_0^* + i\kappa_0 \bar{u}_0^* \bar{q}_0 + \bar{v}_0 (\partial_y \bar{q}_0^*) + \bar{v}_0^* (\partial_y \bar{q}_0), \quad (3.19)$$

$$q_2^\epsilon + (\partial_z \Psi_2^\epsilon)|_{z=0^+} - (\partial_z \Psi_2^\epsilon)|_{z=0^-} = 0, \quad (3.20)$$

$$(\partial_y^2 + \partial_z^2) \Psi_2^\epsilon = 0, \quad (3.21)$$

where the superscript * denotes complex conjugation. A vector $\tilde{\mathcal{C}}_1$ which solves Eqn. 3.12 is presented in Appendix A. The general solution at order ϵ is

$$\mathcal{C}_1 = \tilde{\mathcal{C}}_1 - \{(2\kappa_0)^{-1} (2\partial_x \partial_X A_0) e^{i\kappa_0 x} \bar{\mathcal{C}}_0' + c.c.\}, \quad (3.22)$$

where the prime denotes ∂_κ , and $\bar{\mathcal{C}}_0'$ is given by

$$\bar{\mathcal{C}}_0' = \begin{pmatrix} \bar{v}_0'(y) \\ \bar{q}_0'(y) \\ \bar{\Psi}_0'(y, 0) \\ \bar{\Psi}_0'(y, z) \end{pmatrix} = \begin{pmatrix} (\partial_\kappa \bar{v}_\kappa(y))|_{\kappa=\kappa_0} \\ (\partial_\kappa \bar{q}_\kappa(y))|_{\kappa=\kappa_0} \\ (\partial_\kappa \bar{\Psi}_\kappa(y, 0))|_{\kappa=\kappa_0} \\ (\partial_\kappa \bar{\Psi}_\kappa(y, z))|_{\kappa=\kappa_0} \end{pmatrix}. \quad (3.23)$$

The order $\epsilon^{3/2}$ equation, Eqn. 3.9, can similarly be transformed to

$$\mathcal{L}_0 \tilde{\mathcal{C}}_2 = \mathcal{G} , \quad (3.24)$$

by using Eqn. 3.11. To establish the condition for the existence of a solution $\tilde{\mathcal{C}}_2$ of Eqn. 3.24, the inner product

$$\begin{aligned} (\mathcal{C}_b, \mathcal{C}_a) = & (2\pi/\kappa_0)^{-1} \int_0^{2\pi/\kappa_0} dx \int_{-\infty}^{\infty} dy \{v_b^*(x, y)v_a(x, y) + q_b^*(x, y)q_a(x, y) + \Psi_b^*|_{z=0}\Psi_a|_{z=0}\} \\ & + (2\pi/\kappa_0)^{-1} \int_0^{2\pi/\kappa_0} dx \int_{-\infty}^{\infty} dy \int_{-\infty}^{\infty} dz \{\Psi_b^*(x, y, z)\Psi_a(x, y, z)\} , \end{aligned} \quad (3.25)$$

is employed, where \mathcal{C}_i ($i = a, b$) is

$$\mathcal{C}_i = \begin{pmatrix} v_i(x, y) \\ q_i(x, y) \\ \Psi_i(x, y, z)|_{z=0} \\ \Psi_i(x, y, z) \end{pmatrix} . \quad (3.26)$$

The adjoint operator \mathcal{L}_0^\dagger is determined by integrating $(\mathcal{C}_b, \mathcal{L}_0 \mathcal{C}_a)$ by parts:

$$(\mathcal{C}_b, \mathcal{L}_0 \mathcal{C}_a) = (\mathcal{L}_0^\dagger \mathcal{C}_b, \mathcal{C}_a) + \text{boundary terms} . \quad (3.27)$$

The homogeneous equation $\mathcal{L}_0 \mathcal{C}_a = 0$ with homogeneous boundary conditions, Eqns. 2.14-2.18, will be referred to as the homogeneous ‘‘direct’’ problem. For this case, the left-hand side of Eqn. 3.27 is zero. Some of the boundary terms on the right-hand side of Eqn. 3.27 vanish because of the boundary conditions on the direct variables \mathcal{C}_a . By defining homogeneous boundary conditions for the adjoint quantities \mathcal{C}_b , the remaining boundary terms can be set to zero. This implies that

$$\mathcal{L}_0^\dagger \mathcal{C}_b = 0 , \quad (3.28)$$

or more explicitly

$$\nabla_s^4 v_b - Qq_b = 0 , \quad (3.29)$$

$$-\mathcal{R}_{c0} \partial_x^2 v_b + \Psi_b|_{z=0} = 0 , \quad (3.30)$$

$$\mathcal{R}_{c0} Q \partial_x^2 v_b + \nabla_s^2 q_b + (\partial_z \Psi_b)|_{z=0^+} - (\partial_z \Psi_b)|_{z=0^-} = 0 , \quad (3.31)$$

$$\nabla^2 \Psi_b = 0 . \quad (3.32)$$

Since $\mathcal{L}_0 \neq \mathcal{L}_0^\dagger$, \mathcal{L}_0 is not self-adjoint. The corresponding operator in the Rayleigh-Bénard problem can be made self-adjoint by an appropriate choice of the inner product. [1] This does not appear to be possible in the present case. The boundary conditions on the adjoint quantities are

$$v_b(x, y = \pm \frac{1}{2}) = (\partial_y v_b)(x, y = \pm \frac{1}{2}) = 0, \quad (3.33)$$

$$\Psi_b(x, y = \pm \frac{1}{2}, 0) = q_b(x, y = \pm \frac{1}{2}) = 0, \quad (3.34)$$

$$\Psi_b \rightarrow 0, z \rightarrow \pm \infty. \quad (3.35)$$

As in the direct problem, Dirichlet boundary conditions are employed on the xy plane in the plate electrode configuration with

$$\Psi_b(x, y, 0) = 0, \quad |y| > \frac{1}{2}, \quad (3.36)$$

and mixed boundary conditions are applied in the wire electrode geometry with

$$\partial_z \Psi_b(x, y, z)|_{z=0^+} = 0, \quad |y| > \frac{1}{2}. \quad (3.37)$$

In both cases the relation $\Psi_b(x, y, 0) = \Psi_b|_{z=0}(x, y)$, $|y| \leq 0$, is specified on the film.

The adjoint problem defined by Eqn. 3.28 with boundary conditions Eqns. 3.33-3.37 is satisfied by

$$\mathcal{C}_b = \begin{pmatrix} \bar{v}_{b\kappa_0}(y) \\ \bar{q}_{b\kappa_0}(y) \\ \bar{\Psi}_{b\kappa_0}(y, 0) \\ \bar{\Psi}_{b\kappa_0}(y, z) \end{pmatrix} e^{i\kappa_0 x} = \bar{\mathcal{C}}_{b\kappa_0} e^{i\kappa_0 x}. \quad (3.38)$$

Equations 3.28 and 3.38 are analogous to Eqns. 2.23 and 2.24 in the linear stability problem. The details of the adjoint solution, Eqn. 3.38, are given in Appendix B.

Expanding the product $(\mathcal{C}_b, \mathcal{L}_0 \mathcal{C}_a)$ for the inhomogeneous direct equation $\mathcal{L}_0 \mathcal{C}_a = \mathcal{G}$, with homogeneous boundary conditions Eqns. 2.14-2.18, leads to

$$(\mathcal{C}_b, \mathcal{G}) = (\mathcal{L}_0^\dagger \mathcal{C}_b, \mathcal{C}_a) + \text{boundary terms.} \quad (3.39)$$

The vector \mathcal{C}_b is specified by Eqn. 3.38. The right-hand side of Eqn. 3.39 is zero due to Eqn. 3.28 and the boundary conditions on the direct and adjoint quantities. Equation 3.39 therefore reduces to

$$(\mathcal{C}_b, \mathcal{G}) = 0, \quad (3.40)$$

where

$$\mathcal{G} = \begin{pmatrix} G_1 \\ G_2 \\ G_3 \\ G_4 \end{pmatrix} e^{i\kappa_0 x} + c.c. + \dots \quad (3.41)$$

According to the Fredholm Theorem, Eqn. 3.40 is a necessary and sufficient condition for the existence of a solution of Eqn. 3.24. [15] The remaining terms in Eqn. 3.41 do not contribute to Eqn. 3.40 since they do not depend on $e^{\pm i\kappa_0 x}$. Substituting Eqn. 3.38 and Eqn. 3.41 into Eqn. 3.40 yields

$$\begin{aligned} (\bar{\mathcal{C}}_{b0} e^{i\kappa_0 x}, (G_i) e^{i\kappa_0 x} + c.c.) &= ((\bar{v}_{b0}, \bar{q}_{b0}, \bar{\Psi}_{b0}|_{z=0}, \bar{\Psi}_{b0}) e^{i\kappa_0 x}, (G_1, G_2, G_3, G_4) e^{i\kappa_0 x} + c.c.) \\ &= (2\pi/\kappa_0)^{-1} \int_0^{2\pi/\kappa_0} dx \int_{-\infty}^{\infty} dy \{ \bar{v}_{b0}^* G_1 + \bar{q}_{b0}^* G_2 + \bar{\Psi}_{b0}^*|_{z=0} G_3 \} \\ &\quad + (2\pi/\kappa_0)^{-1} \int_0^{2\pi/\kappa_0} dx \int_{-\infty}^{\infty} dy \int_{-\infty}^{\infty} dz \bar{\Psi}_{b0}^* G_4, \end{aligned} \quad (3.42)$$

where $\bar{\mathcal{C}}_{b0} = \bar{\mathcal{C}}_{b\kappa_0}$, $\bar{v}_{b0} = \bar{v}_{b\kappa_0}$, $\bar{q}_{b0} = \bar{q}_{b\kappa_0}$, and $\bar{\Psi}_{b0} = \bar{\Psi}_{b\kappa_0}$. Completely expanding Eqn. 3.42 gives the amplitude equation

$$F_1 \partial_T A_0 + F_2 A_0 + F_3 (2i\kappa_0 \partial_X)^2 A_0 + F_4 A_0 |A_0|^2 = 0, \quad (3.43)$$

in the slow scales X and T . The coefficients F_i are

$$F_1 = \int_{-1/2}^{1/2} dy \bar{q}_{b0}^* \bar{q}_0, \quad (3.44)$$

$$F_2 = \int_{-1/2}^{1/2} dy \{ -\kappa_0^2 \mathcal{R}_{c0} \bar{v}_{b0}^* (\bar{q}_0 - Q \bar{\Psi}_0|_{z=0}) \}, \quad (3.45)$$

$$\begin{aligned}
F_3 = & \int_{-1/2}^{1/2} dy \{ (2\kappa_0)^{-1} \bar{v}_{b0}^* [2(\partial_y^2 - \kappa_0^2) \bar{v}'_0 - \mathcal{R}_{c0} \bar{q}'_0 + \mathcal{R}_{c0} Q \bar{\Psi}'_0|_{z=0}] - \bar{v}_{b0}^* \bar{v}_0 + (2\kappa_0)^{-1} \bar{q}_{b0}^* \bar{\Psi}'_0|_{z=0} \} \\
& + \int_{-\infty}^{\infty} dy \int_{-\infty}^{\infty} dz (2\kappa_0)^{-1} \bar{\Psi}_{b0}^* \bar{\Psi}'_0 , \tag{3.46}
\end{aligned}$$

$$\begin{aligned}
F_4 = & \int_{-1/2}^{1/2} dy \{ (i\kappa_0)^2 \mathcal{R}_{c0} \bar{v}_{b0}^* [-\bar{q}_0^* (\partial_y \Psi_1^\epsilon|_{z=0}) - 2(\partial_y \bar{q}_0^*) \Psi_1^\epsilon|_{z=0} + 2q_1^\epsilon (\partial_y \bar{\Psi}_0^*|_{z=0}) \\
& + (\partial_y q_1^\epsilon) \bar{\Psi}_0^*|_{z=0} + \bar{q}_0 (\partial_y \Psi_2^\epsilon|_{z=0}) - (\partial_y q_2^\epsilon) \bar{\Psi}_0|_{z=0}] \\
& + \bar{q}_{b0}^* [\frac{1}{2} (\partial_y v_1^\epsilon) \bar{q}_0^* + (2i\kappa_0) \bar{u}_0^* q_1^\epsilon + \bar{v}_0^* (\partial_y q_1^\epsilon) + v_1^\epsilon (\partial_y \bar{q}_0^*) + \bar{v}_0 (\partial_y q_2^\epsilon)] \} , \tag{3.47}
\end{aligned}$$

where the prime denotes ∂_κ . In terms of the fast variables x and t , Eqn. 3.43 is expressed as

$$\tau_0 \partial_t A = \epsilon A + \xi_0^2 \partial_x^2 A - g_0 A |A|^2 , \tag{3.48}$$

such that $A(x, t) = \epsilon^{1/2} A_0(X, T)$, $\tau_0 = -F_1/F_2$, $\xi_0^2 = -4\kappa_0^2 F_3/F_2$, and $g_0 = -F_4/F_2$.

The normalization of the amplitude function in the solution of the $\epsilon^{1/2}$ equation, Eqn. 3.10, is arbitrary. The scale of $A(x, t)$ can be set by requiring

$$Nu - 1 = \langle qv \rangle / \langle \sigma_s E_y \rangle = |A|^2 , \tag{3.49}$$

where

$$\langle \dots \rangle = (2\pi/\kappa_0)^{-1} \int_0^{2\pi/\kappa_0} dx \int_{-1/2}^{1/2} dy (\dots) . \tag{3.50}$$

Note that Nu is the ‘‘Nusselt number’’ for the electroconvection problem, which is defined to be the ratio of the total current density to the conducted current density, spatially averaged.

IV. DISCUSSION AND CONCLUSION

To find the coefficients of the amplitude equation, Eqn. 3.48, we evaluate Eqns. 3.44-3.47 using the numerical techniques described in Refs. [8] and [17]. The y -integrations are performed by the Romberg method. A simple SOR algorithm is employed to solve the Helmholtz equations, Eqns. 3.17, 3.21, and B11, on a $N \times N$ grid in the first quadrant of the yz plane. The solutions in the rest of yz plane follow from symmetry. The double integration in Eqn 3.46 is performed using a 2d trapezoidal rule based on the same grid.

The coefficients are extrapolated such that $N \rightarrow \infty$ and $N_{film}/N \rightarrow 0$, where $2N_{film}$ is the number of grid points across the width of the film. The Fourier series in Eqns. A4, A7, and B9 are expanded up to $l = 29$. Six modes are employed in the solutions Eqns. 2.25-2.27, Eqn. A6, and Eqns. B5-B7, of the linear stability, order ϵ , and adjoint problems, respectively. Including more terms in these series expansions does not significantly change our final results.

The values of τ_0 , ξ_0 , and g_0 are shown in Table I. Only g_0 , the coefficient of the nonlinear term, depends on the normalization of A by the Nusselt number according to Eqn. 3.49. These results can be compared with those obtained independently from the linear stability calculations of Daya *et al.* [8] In the latter approach, the correlation length ξ_0 was derived from the curvature of the neutral curve at κ_0 and the characteristic time τ_0 from the linear growth rate at κ_0 . Both τ_0 and ξ_0 from the linear stability analysis are in good agreement with the present calculation. This provides a useful independent check of our numerical results.

The comparison of our theoretical results with the experiments of Mao *et al.* [7] is difficult at the present time due to the uncertainties in the measurements of the material parameters of the liquid crystal film. For example, to nondimensionalize the experimentally measured value of g_0 , the factor $\epsilon_0^2/\sigma^2 s^2$ must be employed. While the thickness s of the smectic thin film can be measured accurately, the bulk conductivity of the liquid crystal is much less well characterized. Our calculated values of the (Nusselt normalized) value of g_0 are substantially larger than those estimated from experiment [7], but in view of the uncertainty in σ (roughly a factor of 3), no more precise comparison can currently be made. Experiments which will more accurately measure σ and the viscosity η in annular films are presently being performed. [18]

The flow pattern which develops just above onset can be visualized by evaluating the velocity vector field \mathbf{u} on the xy plane. The lowest order x and y components of the field are given by Eqns. A2 and 3.10, respectively. The amplitude function A in these expressions is obtained by solving Eqn. 3.48 for the steady state case with a specified control

parameter ϵ . An example of the resulting vortex pattern is shown in Fig. 2. This may be qualitatively compared with the experimental pattern shown in Fig. 6(b) of Ref. [5]. As above, a quantitative comparison of theoretical and experimental velocities is difficult because of the experimental uncertainty in σ .

In conclusion, a multiple-scales expansion of the basic electrohydrodynamic equations for electroconvection in a suspended fluid film was used to find the lowest order amplitude equation. The set of basic equations were not self-adjoint, necessitating the evaluation of the adjoint eigenfunctions. The coefficients τ_0 , ξ_0 , and g_0 of the resulting Ginzburg-Landau equation were determined by numerical integration. The results of this work can be employed in further studies of the weakly nonlinear phenomena near the onset of electroconvection in suspended smectic films. Of particular interest is the mechanism of wavelength selection [1] and effect of sidewalls on the convection pattern [6,14].

ACKNOWLEDGMENTS

We would like to thank John R. de Bruyn for numerous discussions. This research was supported by the Natural Sciences and Engineering Research Council of Canada.

APPENDIX A:

In this appendix, a method for solving the order ϵ equations, Eqns. 3.14-3.21, is described. Note that the functions $v_1^\epsilon(y)$ and $v_2^\epsilon(y)$ are velocity fields and satisfy Eqn. 2.14, the boundary conditions on v . The quantities $q_1^\epsilon(y)$ and $q_2^\epsilon(y)$ are charge densities. The functions $\Psi_1^\epsilon(y, z)$ and $\Psi_2^\epsilon(y, z)$ are electric potentials and satisfy Eqns. 2.15-2.18, the boundary conditions on Ψ .

To fully specify the order ϵ equations, we relate the x - and y -components of the velocity field. This is accomplished by expanding the incompressibility condition Eqn. 2.2 via the multiple-scales method. At order $\epsilon^{1/2}$, Eqn. 2.2 is

$$\partial_x u_0(x, y) + \partial_y v_0(x, y) = 0, \quad (\text{A1})$$

which can be simplified using the order $\epsilon^{1/2}$ solution for $v_0(x, y)$, Eqn. 3.10, to

$$u_0(x, y) = A_0(X, T)\bar{u}_0(y)e^{i\kappa_0 x} + c.c., \quad (\text{A2})$$

where

$$\bar{u}_0(y) = i\kappa_0^{-1}(\partial_y \bar{v}_0(y)). \quad (\text{A3})$$

The solution of the first set of order ϵ equations, Eqns. 3.14-3.17, begins with Eqn. 3.15. In the linear stability calculation [8], the functions $\bar{v}_0(y)$ and $\bar{q}_0(y)$ are chosen to be even. So $\partial_y \bar{v}_0(y)$ and $\partial_y \bar{q}_0(y)$ are odd. The derivative of the base state charge density $Q(y)$ is even which means that if $v_1^\epsilon(y)$ is odd, then the product $Q(y)v_1^\epsilon(y)$ is also odd. Hence the nonhomogeneous part of Eqn. 3.15 can be expanded in a Fourier sine series

$$-(\partial_y \bar{v}_0(y))\bar{q}_0(y) + \bar{v}_0(y)(\partial_y \bar{q}_0(y)) + Q(y)v_1^\epsilon(y) = \sum_{l=1}^{\infty} b_l \sin(2\pi l y). \quad (\text{A4})$$

The general solution of Eqn. 3.15 is

$$\Psi_1^\epsilon(y, 0) = M \sinh(2\kappa_0 y) - \sum_{l=1}^{\infty} [(2\pi l)^2 + (2\kappa_0)^2]^{-1} b_l \sin(2\pi l y). \quad (\text{A5})$$

The coefficient M is zero due to the boundary condition $\Psi_1^\epsilon(\frac{1}{2}, 0) = 0$. Assuming a trial solution

$$v_1^\epsilon(y) = \sum_{m=1}^N E_m S_m(y), \quad (\text{A6})$$

where S_m is the odd Chandrasekhar function [16] with $E_m = 1$ for $m = 1, \dots, N$, yields the coefficients b_l in Eqn. A4. Equation A5 and the boundary conditions Eqns. 2.16-2.18 determine $\Psi_1^\epsilon(y, z)$ via the Helmholtz equation, Eqn. 3.17, which is solved by a numerical relaxation method. The function $q_1^\epsilon(y)$ is found by numerical differentiation of $\Psi_1^\epsilon(y, z)$ in Eqn. 3.16. Then $q_1^\epsilon(y)$ and $\Psi_1^\epsilon(y, 0)$ are substituted into Eqn. 3.14 to calculate a new estimate of $v_1^\epsilon(y)$. This process is repeated until $v_1^\epsilon(y)$, $q_1^\epsilon(y)$, and $\Psi_1^\epsilon(y, z)$ are self-consistently determined.

In the second set of order ϵ equations, Eqns. 3.18-3.21, Eqn. 3.18 and the boundary conditions Eqn. 2.14 indicate that $v_2^\epsilon(y) = 0$. The right-hand side of Eqn. 3.19, simplified via Eqn. A3, is an odd function and can be expanded in a Fourier sine series. The general solution of Eqn. 3.19 is

$$\Psi_2^\epsilon(y, 0) = - \sum_{l=1}^{\infty} (2\pi l)^{-2} a_l \sin(2\pi l y) . \quad (\text{A7})$$

The variable $\Psi_2^\epsilon(y, z)$ is specified by solving the Laplace equation, Eqn. 3.21, by a relaxation method, subject to Eqn. A7 and the boundary conditions Eqns. 2.16-2.18. The function $q_2^\epsilon(y)$ is numerically calculated via Eqn. 3.20.

APPENDIX B:

The solution of the adjoint problem, Eqns. 3.28-3.37, is discussed in this section. Substitution of the vector $\bar{\mathcal{C}}_{b\kappa_0}$, Eqn. 3.38, into Eqns. 3.29-3.32 gives

$$(\partial_y^2 - \kappa_0^2)^2 \bar{v}_{b\kappa_0} - Q \bar{q}_{b\kappa_0} = 0 , \quad (\text{B1})$$

$$\kappa_0^2 \mathcal{R}_{c0} \bar{v}_{b\kappa_0} + \bar{\Psi}_{b\kappa_0}|_{z=0} = 0 , \quad (\text{B2})$$

$$-\kappa_0^2 \mathcal{R}_{c0} Q \bar{v}_{b\kappa_0} + (\partial_y^2 - \kappa_0^2) \bar{q}_{b\kappa_0} + (\partial_z \bar{\Psi}_{b\kappa_0})|_{z=0^+} - (\partial_z \bar{\Psi}_{b\kappa_0})|_{z=0^-} = 0 , \quad (\text{B3})$$

$$(\partial_y^2 + \partial_z^2 - \kappa_0^2) \bar{\Psi}_{b\kappa_0} = 0 . \quad (\text{B4})$$

To simplify the notation, let $\bar{v}_{b0} = \bar{v}_{b\kappa_0}$, $\bar{q}_{b0} = \bar{q}_{b\kappa_0}$, and $\bar{\Psi}_{b0} = \bar{\Psi}_{b\kappa_0}$. The functions $\bar{v}_{b0}(y)$, $\bar{q}_{b0}(y)$, and $\bar{\Psi}_{b0}(y, z)$ are expanded as

$$\bar{v}_{b0}(y) = \sum_{m=1}^{\infty} B_m \bar{v}_{b0m}(y) , \quad (\text{B5})$$

$$\bar{q}_{b0}(y) = \sum_{m=1}^{\infty} B_m \bar{q}_{b0m}(y) , \quad (\text{B6})$$

$$\bar{\Psi}_{b0}(y, z) = \sum_{m=1}^{\infty} B_m \bar{\Psi}_{b0m}(y, z) , \quad (\text{B7})$$

where $\bar{v}_{b0m}(y)$, $\bar{q}_{b0m}(y)$, and $\bar{\Psi}_{b0m}(y, z)$ satisfy the adjoint boundary conditions, Eqns. 3.33-3.37.

With the solutions Eqns. B5-B7, Eqn. B1 implies that

$$(\partial_y^2 - \kappa_0^2)^2 \bar{v}_{b0m}(y) - Q(y) \bar{q}_{b0m}(y) = 0 . \quad (\text{B8})$$

Since $\bar{q}_{b0m}(y)$ must satisfy $\bar{q}_{b0m}(y = \pm \frac{1}{2}) = 0$, let $\bar{q}_{b0m}(y) = \cos((2m-1)\pi y)$. The product of $Q(y)$ and $\cos((2m-1)\pi y)$ is even and can be represented by a Fourier cosine series. The general solution of Eqn. B8 is

$$\bar{v}_{b0m}(y) = M_1 \cosh(\kappa_0 y) + M_2 y \sinh(\kappa_0 y) + \sum_{l=0}^{\infty} [(2\pi l)^2 + \kappa_0^2]^{-2} b_{ml} \cos(2\pi l y) , \quad (\text{B9})$$

where the constants M_1 and M_2 are specified by the boundary conditions $\bar{v}_{b0m}(y = \pm \frac{1}{2}) = (\partial_y \bar{v}_{b0m})(y = \pm \frac{1}{2}) = 0$ to be

$$M_1 = -2(\kappa_0 + \sinh(\kappa_0))^{-1} [\sinh(\kappa_0/2) + (\kappa_0/2) \cosh(\kappa_0/2)] \sum_{l=0}^{\infty} (-1)^l [(2\pi l)^2 + \kappa_0^2]^{-2} b_{ml} ,$$

$$M_2 = -2(\kappa_0 + \sinh(\kappa_0))^{-1} [-\kappa_0 \sinh(\kappa_0/2)] \sum_{l=0}^{\infty} (-1)^l [(2\pi l)^2 + \kappa_0^2]^{-2} b_{ml} .$$

Substitution of Eqns. B5-B7 into Eqn. B2 and Eqn. B4 yields

$$\bar{\Psi}_{b0m}(y, 0) = -\kappa_0^2 \mathcal{R}_{c0} \bar{v}_{b0m}(y) , \quad (\text{B10})$$

and

$$(\partial_y^2 + \partial_z^2 - \kappa_0^2) \bar{\Psi}_{b0m}(y, z) = 0 . \quad (\text{B11})$$

The latter is a Helmholtz equation subject to the adjoint boundary conditions Eqns. 3.36 and 3.37, with $\bar{\Psi}_{b0m}(y, 0)$, $|y| \leq \frac{1}{2}$, given by Eqn. B10. Equation B11 is solved by a numerical relaxation method.

Using Eqns. B5-B7 to expand Eqn. B3 leads to

$$\sum_m B_m [-\kappa_0^2 \mathcal{R}_{c0} Q \bar{v}_{b0m} + (\partial_y^2 - \kappa_0^2) \bar{q}_{b0m} + (\partial_z \bar{\Psi}_{b0m})|_{z=0^+} - (\partial_z \bar{\Psi}_{b0m})|_{z=0^-}] = 0 . \quad (\text{B12})$$

Since $\bar{v}_{b0m}(y)$, $\bar{q}_{b0m}(y)$, and $\bar{\Psi}_{b0m}(y, z)$ are known functions, Eqn. B12 implies that the coefficients B_m vanish unless the compatibility condition

$$\left\| T_{nm} \right\| = \left\| \int_{-1/2}^{1/2} dy [-\kappa_0^2 \mathcal{R}_{c0} Q \bar{q}_{b0n} \bar{v}_{b0m} + \bar{q}_{b0n} (\partial_y^2 - \kappa_0^2) \bar{q}_{b0m} + 2\bar{q}_{b0n} (\partial_z \bar{\Psi}_{b0m})|_{z=0+}] \right\| = 0 , \quad (\text{B13})$$

is satisfied. Note that the relation $(\partial_z \bar{\Psi}_{b0m})|_{z=0^-} = -(\partial_z \bar{\Psi}_{b0m})|_{z=0^+}$, which is analogous to the discontinuity in the electric field $\partial_z \bar{\Psi}_{0m}$ across the two surfaces of the film in the direct problem, is used to derive Eqn. B13. In Eqn. B13, the values of κ_0 and \mathcal{R}_{c0} are fixed to be those obtained from the linear stability analysis. The coefficients B_m are determined by the matrix equation

$$T_{nm} B_m = 0 , \quad (\text{B14})$$

where T_{nm} is given in Eqn. B13. These coefficients are then substituted into Eqns. B5-B7 to generate $\bar{v}_{b0}(y)$, $\bar{q}_{b0}(y)$, and $\bar{\Psi}_{b0}(y, z)$. This specifies $\bar{\mathcal{C}}_{b\kappa_0}$ and the general solution vector \mathcal{C}_b , Eqn. 3.38.

REFERENCES

- [1] M.C. Cross and P.C. Hohenberg, *Rev. Mod. Phys.*, **65**, 851 (1993).
- [2] G. Ahlers, in *Lectures in the Sciences of Complexity*, edited by D. Stein (Addison-Wesley, Reading, 1989), p. 175.
- [3] L. Kramer and W. Pesch, in *Pattern Formation in Liquid Crystals*, A. Buka and L. Kramer eds. (Springer, New York, 1995), and *Annual Rev. Fluid Mech.*, **27**, 515 (1995).
- [4] S.W. Morris, J.R. de Bruyn, and A.D. May, *Phys. Rev. Lett.*, **65**, 2378 (1990); *J. Stat. Phys.*, **64**, 1025 (1991).
- [5] S.W. Morris, J.R. de Bruyn, and A.D. May, *Phys. Rev. A*, **44**, 8146 (1991).
- [6] S.S. Mao, J.R. de Bruyn, Z.A. Daya, and S.W. Morris, *Phys. Rev. E*, **54**, R1048 (1996).
- [7] S.S. Mao, J.R. de Bruyn, and S.W. Morris, to be published *Physica A* (1997).
- [8] Z.A. Daya, S.W. Morris, and J.R. de Bruyn, to be published *Phys. Rev. E* (1997).
- [9] A. Becker, S. Ried, R. Stannarius, and H. Stegemeyer, unpublished.
- [10] S. Ried, H. Pleiner, W. Zimmermann, and H. Brand, *Phys. Rev. E*, **53**, 6101 (1996).
- [11] S. Faetti, L. Fronzoni, and P. Rolla, *J. Chem. Phys.*, **79**, 5054 (1983).
- [12] P. Manneville, *Dissipative Structures and Weak Turbulence* (Academic, San Diego, 1990).
- [13] M.C. Cross, P.G. Daniels, P.C. Hohenberg, and E.D. Siggia, *Phys. Rev. Lett.*, **45**, 898 (1980); M.C. Cross, P.C. Hohenberg, P. Daniels, and E.D. Siggia, *J. Fluid Mech.*, **127**, 155 (1983).
- [14] V.B. Deyirmenjian, Z.A. Daya, and S.W. Morris, unpublished.
- [15] I. Stakgold, *Green's Functions and Boundary Value Problems* (New York: Wiley, 1979).

- [16] S. Chandrasekhar, *Hydrodynamic and Hydromagnetic Stability* (Oxford: Clarendon, 1961).
- [17] W. H. Press, S. A. Teukolsky, W. T. Vetterling, and B. P. Flannery, *Numerical Recipes in C*, (Cambridge University Press, Cambridge, 1992).
- [18] Z. A. Daya, S.W. Morris, and J. R. de Bruyn, unpublished.

TABLES

TABLE I. Numerical results

	Nonlinear Analysis	Linear Stability
Wire Electrode Geometry		
critical wavenumber, κ_0	4.7467	4.744
critical control parameter, \mathcal{R}_{c0}	76.855	76.77
correlation length, ξ_0	0.28484	0.2843
time scale, τ_0	0.35072	0.351
nonlinear coupling, g_0	1.74602	-
Plate Electrode geometry		
critical wavenumber, κ_0	4.2239	4.223
critical control parameter, \mathcal{R}_{c0}	91.855	91.84
correlation length, ξ_0	0.29743	0.2975
time scale, τ_0	0.37155	0.372
nonlinear coupling, g_0	2.8424	-

FIGURES

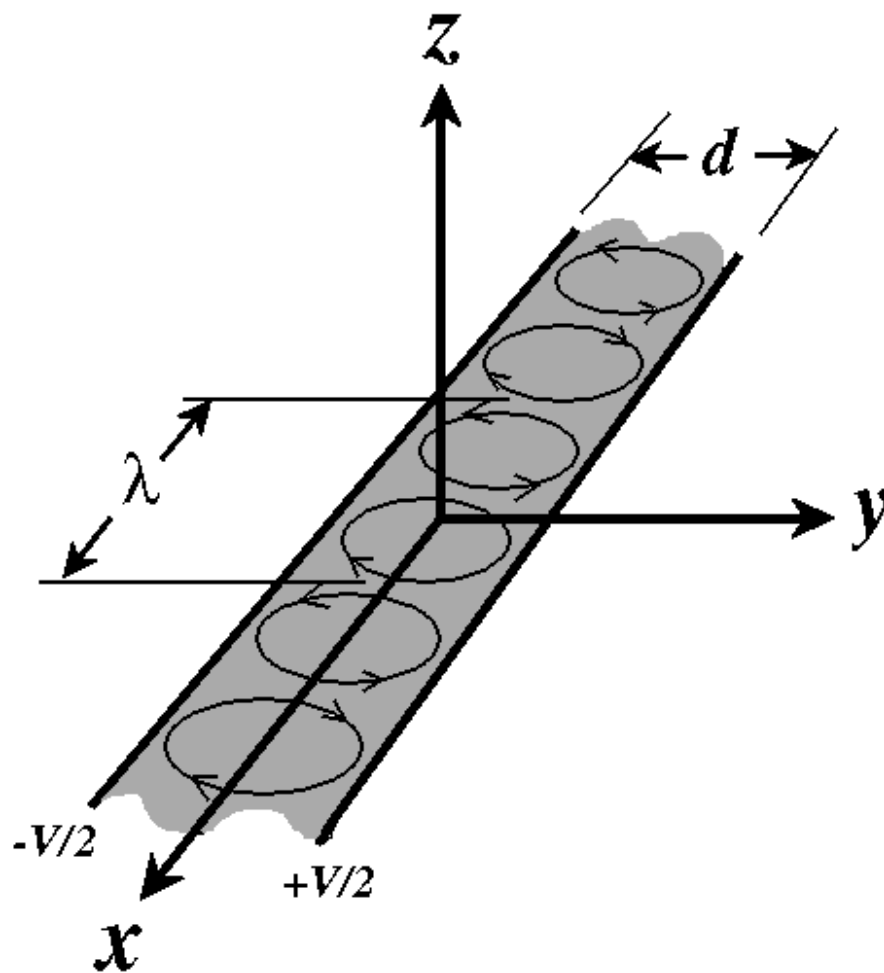


FIG. 1. Schematic of film geometry and coordinate system. The wire electrode configuration is shown. The vortex pair periodicity is $\lambda = 2\pi d/\kappa$, where d is the film width. The thickness s of the film (not shown) is such that $s \ll d$.

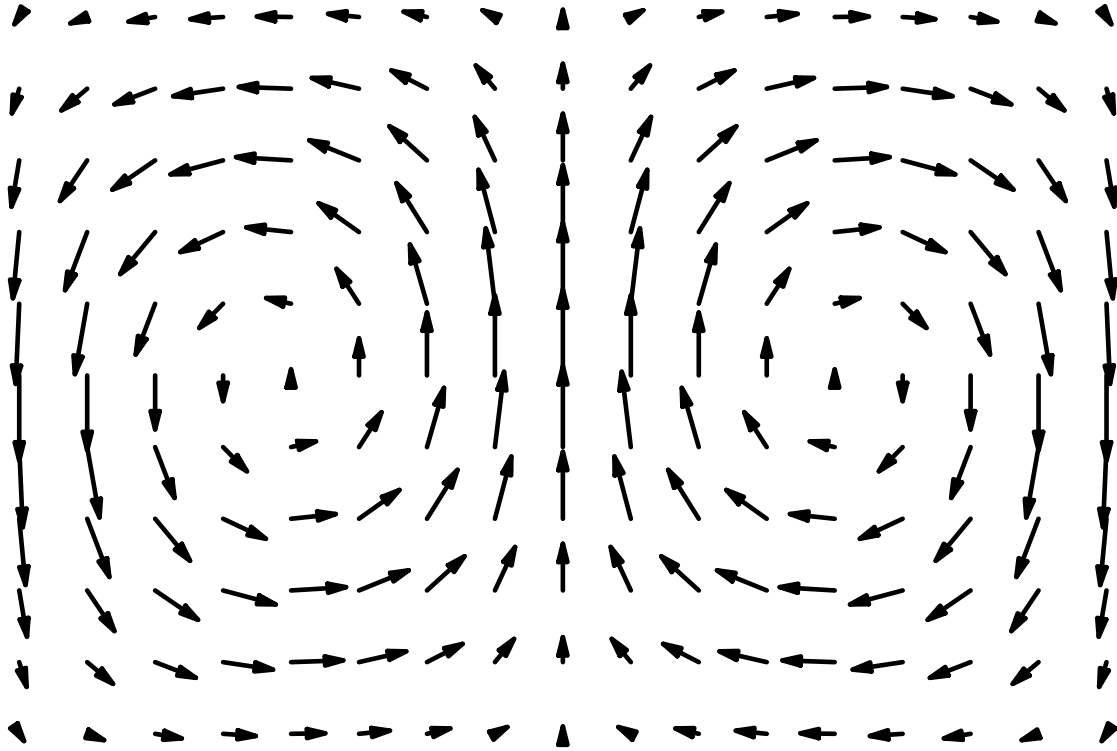


FIG. 2. Vortex pattern just above onset. The dimensionless velocity must be scaled by $s\sigma/\epsilon_0$, where s , σ , and ϵ_0 are the film thickness, bulk conductivity, and permittivity of free space, respectively. Here we plot the vector velocity field for wire electrodes with control parameter $\epsilon = 0.1$. Using $s = 142$ nm and $\sigma = 2.0 \times 10^{-7}$ (Ωm) $^{-1}$, which are typical values for smectic films, gives $s\sigma/\epsilon_0 = 3.2$ mm/s. The magnitude of the velocity at the centre of the figure is approximately equal to 2.4 mm/s.